(Received 21 August 2025, Accepted 26 September 2025, Scheduled 30 October 2025)

A Low-Profile UWB Monopole Antenna and High-Isolated UWB-MIMO Antenna for Wireless Communications Networks

Ibrahime H. Nejdi[1,*], Mohamed Marzouk[2], Mustapha A. Lafkih[1], Seddik Bri[3], Jamal A. Nasir[4], Zahriladha Zakaria[5,*], and Ahmed J. A. Al-Gburi[5]

[1]*Automatic and Energy Conversion (AEC), Faculty of Science and Technology Sultan Moulay Slimane University, Beni-Mellal, Morocco*
[2]*Microelectronics, Embedded Systems and Telecommunications (MiSET) Faculty of Sciences and Technology, Sultan Moulay Slimane University, Beni-Mellal, Morocco*
[3]*Material and Instrumentations Group, Electrical Engineering Department, Moulay Ismail University, Morocco*
[4]*Department of Electrical Engineering, Faculty of Engineering & Technology, Gomal University, Pakistan*
[5]*Center for Telecommunication Research & Innovation (CeTRI) Fakulti Teknologi Dan Kejuruteraan Elektronik Dan Komputer (FTKEK) Universiti Teknikal Malaysia Melaka (UTeM), Hang Tuah Jaya, Durian Tunggal, Melaka 76100, Malaysia*

ABSTRACT: This study proposes a space-efficient ultra-wideband (UWB) monopole antenna engineered for superior gain and performance. The innovative design, modeled and analyzed using HFSS software, involves etching the resonator onto one side of an affordable FR4 substrate. The manufactured antenna features an extended impedance bandwidth, achieved by incorporating "E" and "inverted E" shaped slots on the patch, an irregular hexagonal substrate structure, and a slotted partial ground plane. Covering a frequency range from 2.5 to 11.1 GHz, the patch achieves a maximum gain exceeding 7.9 dB and an efficiency of 98%. Parametric analyses based on numerical simulations evaluate the impact of design elements, such as slots on the resonator and ground plane, and cuts in the substrate. The excellent match between simulated and measured data verifies the antenna's performance across multi-band environments. The article concludes by introducing a second antenna, designed through the symmetrical integration of four prototypes of the suggested antenna. Mutual coupling between elements is reduced through the use of an orthogonal, four-directional staircase structure, and a defective ground is intentionally left unconnected. This new antenna covers an impedance spectrum from 2.42 to 12 GHz, with a gain of 12.77 dB, an efficiency of up to 98%, and a voltage standing wave ratio (VSWR) ranging between 1 and 2. Overall, the article emphasizes the design, optimization, and application of UWB antennas, highlighting their performance and suitability for various wireless communication scenarios.

1. INTRODUCTION

Over the years, it has become highly desirable to have low-profile, compact, and wideband antennas with multiband characteristics to meet the requirements of modern wireless communication systems. The rapid and remarkable development of most of these systems over the past decade has underscored this need. In 2002, the United States Federal Communication Commission (FCC) allocated the UWB spectrum from 3.1 to 10.6 GHz for commercial applications of UWB communication systems [1].

UWB antennas are highly versatile and find utility in a wide range of applications, spanning from high-precision localization [2] to high-resolution radar imaging [3], high-speed communications [4], automotive safety [5], the Internet of Things (IoT) [6], environmental monitoring, security, and defense, as well as consumer applications like augmented reality. The versatility of UWB antennas makes them an essential tool adopted in various industries [7]. Furthermore, the UWB spectrum is characterized by an extremely low power spectral density, making it less susceptible to interference [8]. Additionally, UWB radiation has a virtually negligible impact on the human body, positioning it as one of the most promising technologies for global wearable applications. Consequently, for effective wireless transmission and reception, portable systems necessitate the integration of UWB portable antennas. The limited communication range of UWB is due to its low spectral density. However, this feature necessitates the use of high-gain antennas with relatively stable radiation characteristics [9]. Various shapes and sizes of UWB monopole patches with different substrate types have been explored by researchers for various applications [10–16]. Characteristics such as reduced size, low profile, high radiation efficiency, lightweight design, and ease of integration into communication devices make unipolar planar patches an attractive option for UWB transceiver systems [10]. In [11], there is a description of a planar patch antenna fed by a coplanar waveguide, offering UWB circular polarization. In [12], Li and co-authors utilized a coplanar patch with a conical slot to achieve UWB operation. They introduced two innovative anti-spiral shapes at the end of the slot to increase the electrical aperture and reduce reflection power. To achieve UWB functionality and operate within the ISM band (2.45 GHz), the authors of [14] employed a dual-spectrum split-

* Corresponding authors: Ibrahime Hassan Nejdi (ibrahime.nejdi@usms.ma); Zahriladha Zakaria (zahriladha@utem.edu.my).

ring antenna. Ref. [17] introduces a compact planar monopole antenna with a quadrilateral shape, fed by a coplanar waveguide, specifically designed for UWB applications. However, UWB patches face the inherent challenge of limited radiation range at shorter distances due to reduced transmission power, as highlighted by the FCC.

The challenges stemming from short-range and low-power transmission can be bypassed through the use of MIMO (Multiple Input, Multiple Output) technology in conjunction with UWB. This approach involves employing multiple radiating elements for wireless signal transmission and reception. The benefits of utilizing a MIMO antenna rather than a monopole antenna will be described next for UWB devices, as follows:

- Transmission Reliability: The spatial diversity provided by MIMO antennas contributes to improving transmission reliability. By leveraging multiple propagation paths, they mitigate the effects of multipath, signal attenuation, and interference, ensuring more robust communication.
- Improving Distance Resolution: MIMO antennas can improve distance resolution, a crucial aspect for precise indoor localization applications. By exploiting the differences in signal arrival times between the antennas, they enable more precise localization of UWB devices.
- Management of Spatial Multiplexing: MIMO configurations enable spatial multiplexing and can utilize the antenna arrays to direct separate data users with directional beams. This also better utilizes the spectral efficiency and capacity of a UWB system.
- Interference Mitigation: MIMO antennas can be designed to mitigate high or low-level interference in the presence of significant noise or competing wireless systems. Improved signal quality can be achieved using optimized beamforming for the UWB system with minimized interference even in relatively crowded settings.

However, the major challenge encountered with MIMO antennas lies in the high coupling between the resonators. To mitigate the coupling between elements in wideband planar MIMO antennas, various approaches have been explored [18–35] including the use of electromagnetic bandgap (EBG) structures and other decoupling techniques, as documented in References [18–21]. Additionally, the authors of [22–24] introduced dual-port MIMO antennas incorporating split-ring resonators (SRRs), showcasing a significant improvement in isolation between elements. In [25], a UWB MIMO configuration utilizing eight 3D-shaped resonator elements was reported. To address the issue of mutual coupling, the authors positioned the resonant elements in both horizontal and vertical orientations. A dual-polarization antenna for UWB signals was developed by Maurya N. K. and Bhattacharya R. in [30]. In this design, the authors positioned the antenna elements orthogonally, aiming to enhance isolation between them and achieve polarization diversity. In [27], the authors introduced F-shaped stubs in the common ground plane of their work to enhance the isolation between the resonant elements of the MIMO antenna. In [28], an extruded T-shaped stub is incorporated at the rectangular ground plane to improve isolation. Additionally, [29] proposes the use of four-way staircase-shaped decoupling and the technique and multi-slit and multi-slot techniques to reduce the mutual couplings between the rayonnant element.

In this article, two UWB antennas are proposed to provide a typical solution for short-range wireless communications due to their ability to transmit signals over a broad frequency range and low power consumption in both transmission and reception. The article introduces a compact UWB monopole antenna characterized by high efficiency and high gain. This innovative design relies on the High Frequency Structure Simulator (HFSS) software for modeling and analyzing the multiple slots used on the patch and the ground plane. The manufactured UWB antenna covers a frequency range from 2.5 to 11.1 GHz, with a maximum gain exceeding 7.9 dB and an efficiency reaching 98%. Several parametric analyses based on numerical simulations are conducted to achieve an optimal design.

The article concludes with an improvement in antenna performance by applying the MIMO technique. To significantly reduce mutual coupling between antenna elements, a structure in the form of a distinct, orthogonal, and symmetrical four-directional staircase with a defective ground, is intentionally left unconnected. This innovative design enables the antenna to operate across an impedance spectrum ranging from 2.42 to 12 GHz, with a maximum gain of 12.77 dB and an efficiency reaching 98%.

2. ANTENNA DESIGN

Figure 1 illustrates the schematic layout of the suggested UWB patch. The design of this patch involves a printed monopole featuring two "E" and "inverted E" shaped slots at the resonator level, as well as a rectangular slot on the ground plane. It is mounted on an irregular polygon-shaped, cost-effective FR4 substrate with volume of $1101.38\,\text{mm}^2 \times 1.6\,\text{mm}$ and a dielectric constant of 4.4. The monopole antenna is fed through a $50\,\Omega$ impedance feed line with a width referred to as "W_F" and a length denoted as "L_f". The HFSS computer simulator was utilized to design and simulate this antenna. Table 1 details the dimensions obtained through optimization. In this study, selecting a circular radiating structure aims to provide a UWB operation while occupying less space than conventional radiating antennas.

TABLE 1. Units for magnetic properties.

Parameters	L_s	W_s	R	W_f	L_f
Values (mm)	28.7	31.25	13	3.95	11.15
Parameters	F_1	F_2	F_3	L_1	L_2
Values (mm)	18	12.5	7.5	13.13	9.94
Parameters	L_3	L_4	L_5	L_6	L_7
Values (mm)	11.25	3	2.25	3	12.69

2.1. Diverse Phases in the Design Process

Figure 2 displays the distinct design stages of the designed monopole presented in this work. The transmission line method is adopted for the design of the initiator patch illustrated in Fig. 2(a), and it is a circular monopole antenna of radius R.

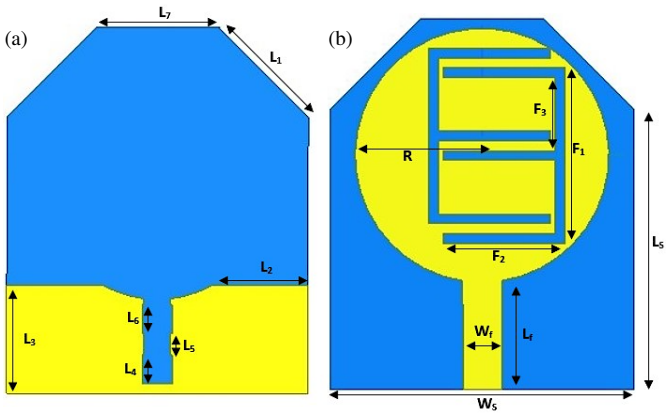

FIGURE 1. UWB patch, (a) front view, (b) rear view.

The resonance frequency f_o of the circular radiator is determined using (1) provided by Reference [36]:

$$f_0 = 1.8412 \times c/4\pi R_{eff}\sqrt{\varepsilon_r} \quad (1)$$

where "c" represents the light speed, and "R_{eff}" is the effective radius of the radiator, which is calculated by (2):

$$R_{eff} = R\sqrt{1 + \frac{2h}{\pi\varepsilon_r R_0}\left(\ln\left(\frac{\pi R}{2h}\right) + 1.7726\right)} \quad (2)$$

In this context, "h" represents the substrate's thickness, "R" the resonator's radius, and "ε_r" the dielectric constant of the substrate. The initiator patch's radius is computed at the resonant frequency of 3.58 GHz. Then, in the first step, an "E"-shaped slot was cut from the resonator, as shown in Fig. 2(b), to improve the antenna characteristics. Furthermore, in the second step, as illustrated in Fig. 2(c), an inverted "E"-shaped slot was cut from the resonator created in the first step. Two cuts were made on the substrate in the third step, which presents the proposed antenna. These modifications are made to achieve Ultra-Wideband (UWB) operation.

2.2. Antenna Design Approach

Figure 3 displays the S_{11} characteristics in a way that reflects the step-by-step design progress. The Step 0 patch presents a monopole circular antenna, which can operate with a bandwidth of 0.17 and 0.65 GHz in the frequency ranges of 3.55 to 3.72 GHz and 6.0 to 6.65 GHz, respectively. Starting with the modification to the antenna in Step 1, the operating ranges have seen a significant improvement. However, at this point, the antenna exhibits performance over four impedance bands: 0.1 GHz, 1.84 GHz, 1.56 GHz, and 1.11 GHz. While displaying a maximum gain of 5.01 dB. Thus, the insertion of the two "E"-shaped and inverted "E"-shaped slots in the antenna in the penultimate step allowed for the achievement of dual-band operation with a bandwidth of 3.13 GHz and 2.98 GHz in the operating ranges of [2.47–5.60] GHz and [6.90–9.88] GHz, respectively. It is evident that Step 3, which presents the proposed antenna with a substrate modification, has contributed to improving the antenna's matching and expanding the operational frequency range. This modification has increased operating bandwidth, covering all the desired frequencies intended for wireless communication applications. According to simulations, the antenna is now capable of operating in UWB mode over a frequency range from 2.57 GHz to 11.10 GHz. This operating frequency range ensures UWB operation with better gain and high efficiency that reaches 7.98 dB and 98%, representing a promising development for wireless communication applications. The antenna provides a diversity of use cases with remarkable versatility. They include applications such as high-accuracy localization, high-resolution radar imaging, high-speed communication, road safety, health monitoring, the Internet of Things (IoT), environmental monitoring, security, defense, and consumer-oriented uses like augmented reality.

In the context of UWB operation, the introduction of the "E" and inverted "E" shaped slots plays a crucial role in bandwidth enhancement. These slots perturb the surface current distribution on the radiating patch, effectively increasing the electrical path length and enabling the excitation of additional resonant modes. The interaction between these newly introduced resonances and the fundamental mode leads to improved impedance matching over a wider frequency range. As a result, the antenna achieves an expanded operational bandwidth while maintaining stable radiation characteristics across the UWB spectrum. Moreover, modifying the substrate in the proposed antenna enhances impedance matching and broadens the operational frequency range by adjusting the effective dielectric constant, controlling surface wave propagation, and influencing resonance behavior. Changes to substrate material improve impedance matching across frequencies, while structural modifications help suppress unwanted surface waves that can otherwise cause mismatches. These adjustments optimize current distribution, allowing the antenna to support multiple resonant frequencies, and improve radiation efficiency by guiding electromagnetic fields effectively, collectively expanding the bandwidth and operational range.

2.3. Circuit Model for Patch Antennas

The equivalent circuit for antennas is a simplified representation of the antenna using passive electrical components such as resistances, inductances, and capacitances. This representation facilitates the analysis and understanding of the antenna's behavior in the electrical domain. The main elements of the equivalent circuit include:

- Complex input impedance: Comprising resistance and reactance, it represents the response of the antenna.
- Radiation resistance represents the amount of power dissipated in the form of electromagnetic radiation.
- Loss resistance represents internal losses due to effects such as the ohmic resistance of materials.
- Capacitance and inductance reactive components were modeling the energy storage properties of the antenna.

The equivalent circuit allows for the analysis of the antenna's impedance as a function of frequency, which is essential for impedance matching and performance optimization. Additionally, circuit simulation tools use these equivalent models to predict the behavior of antennas under various conditions.

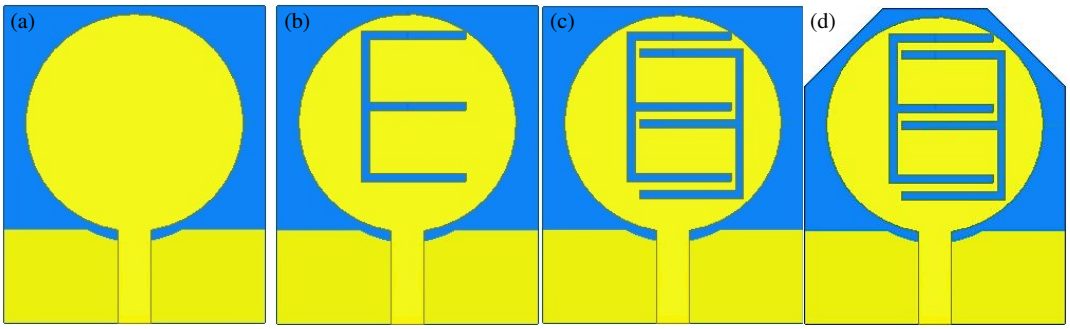

FIGURE 2. Distinct design stages of the suggested UWB patch, (a) initiator antenna (Step 0), (b) first "E" shaped slot (Step 1), (c) second slot in the shape of an inverted "E" (Step 2), (d) suggested UWB antenna.

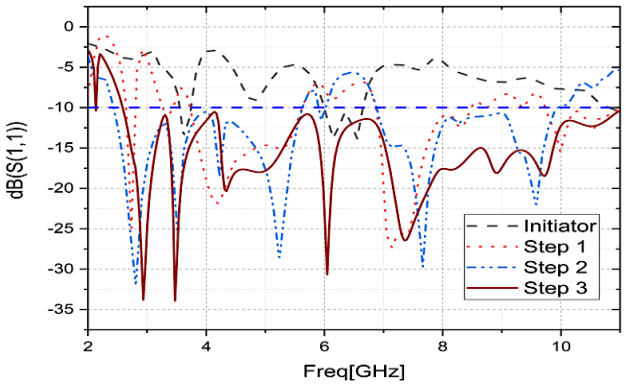

FIGURE 3. Distinct stages S_{11} of the suggested UWB antenna.

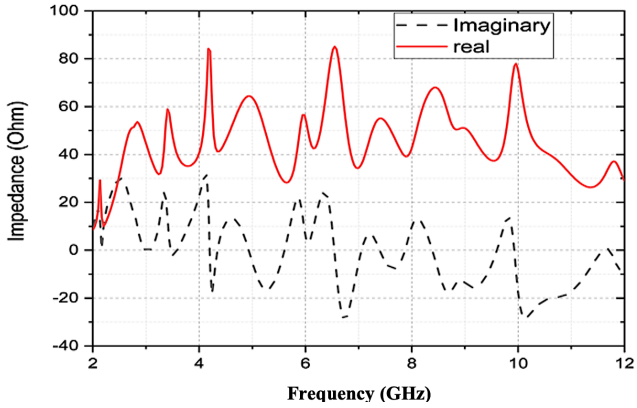

FIGURE 4. Simulated input impedance.

The input impedance of a patch is a complex quantity that varies with geometry, environment, and frequency. Precision in representing this input impedance can be achieved by using equivalent circuits comprising localized elements. In their works cited under References [37] and [38], the authors developed the equivalent model of a broadband monopole in an aerial environment. Broadband antennas can be considered multiband antennas and are represented by an LC input cell coupled in series with N cells (parallel RLC circuits). Figs. 4 and 5 sequentially present the input impedance and the equivalent circuit. "N" is defined by the number of local maxima the input impedance gives. In this situation, eight local maxima are observed, requiring the calculation of eight cells. Each cell's constituent elements (R_i, L_i, C_i) $(i = 1, 2, ..., N)$ are derived from the real part of the input impedance plot. Additionally, the components of the input cell (C_0 and L_0) are determined based on the imaginary part of the input impedance plot. The detailed steps for deriving the equivalent model of the antenna patch in an aerial environment are extensively explained in References [37] and [38]. The general expression for the input impedance of the equivalent circuit is written by (3). Table 2 presents the equivalent circuit parameters for the antenna.

$$Z_{eq} = j2\pi f L_0 + \frac{1}{j2\pi f C_0} + \sum_{i=1}^{N} \left(\frac{1}{R_i} + \frac{1}{j2\pi f L_i} + j2\pi f C_i \right)^{-1} \quad (3)$$

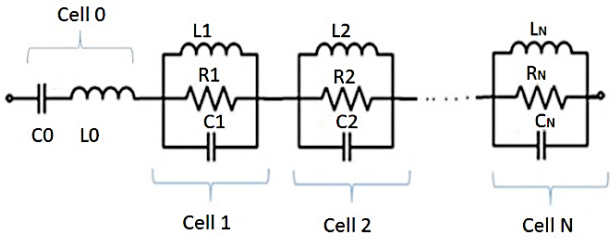

FIGURE 5. Configuration of the equivalent circuit for antennas.

2.4. Parametric Analysis of the Suggested UWB Patch

After various optimizations based on different parameters, the proposed design has been finalized. In this section, a parametric analysis using the HFSS simulator was conducted. The antenna's performance is closely tied to the dimensional parameters of the suggested antenna. Variations in these parameters lead to substantial changes in antenna performance. Optimal dimensions for the suggested antenna can be deduced through parametric studies, ensuring its efficient operation by maximizing its attributes.

2.4.1. Effect of the Feed Line Width (W_f)

The study of the influence of feed line width on reflection coefficient, while keeping other parameters of the proposed antenna dimensions constant, is shown in Fig. 6(a). According

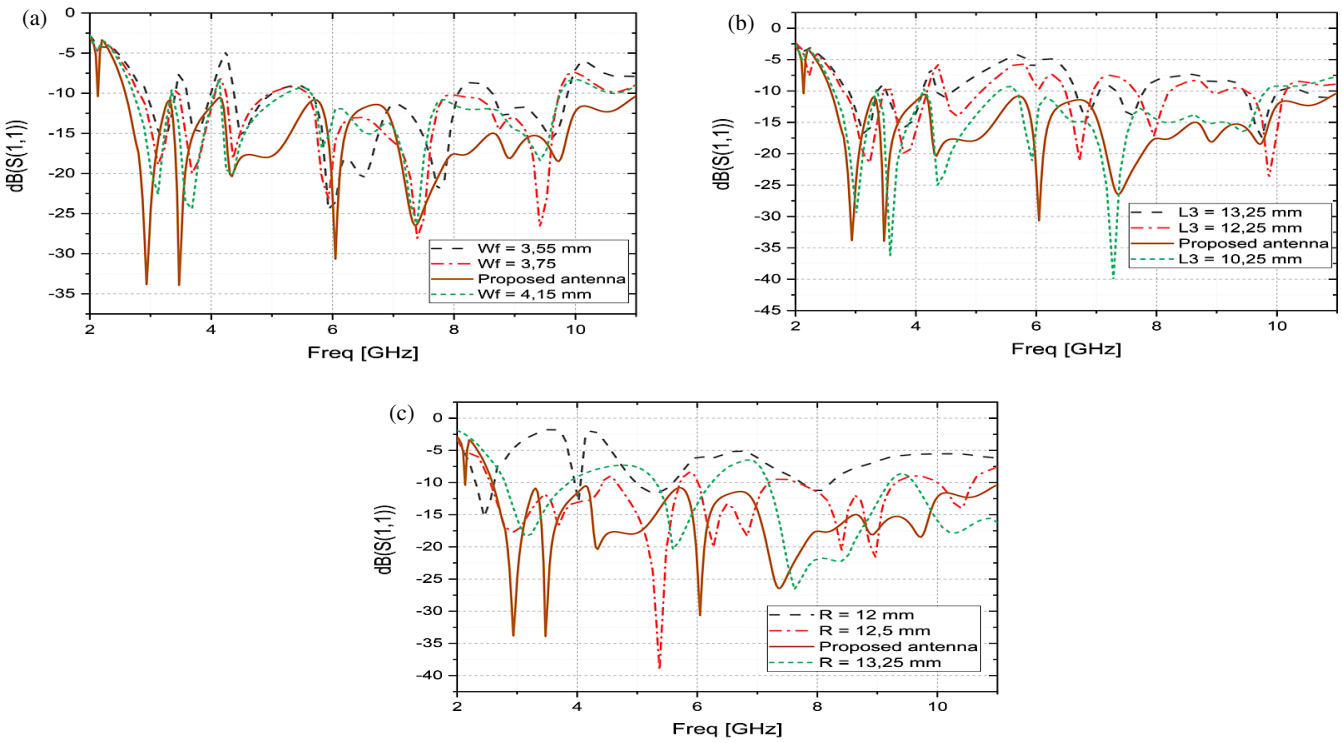

FIGURE 6. S_{11} plot for (a) S_{11} W_f, (b) S_{11} L_3, (c) S_{11} R.

TABLE 2. Equivalent circuit parameters.

Circuit parameters	C_0 (pF)	L_0 (nH)	R_1 (Ω)	C_1 (pF)	L_1 (nH)	R_2 (Ω)
Value	19.19	0.46	53.62	15.32	0.0026	58.99
Circuit parameters	C_2 (pF)	L_2 (nH)	R_3 (Ω)	C_3 (pF)	L_3 (nH)	R_4 (Ω)
Value	11.72	0.18	84.24	14.32	0.10	64.43
Circuit parameters	C_4 (pF)	L_4 (nH)	R_5 (Ω)	C_5 (pF)	L_5 (nH)	R_6 (Ω)
Value	3.03	0.34	85.09	4.97	0.12	55.13
Circuit parameters	C_6 (pF)	L_6 (nH)	R_7 (Ω)	C_7 (pF)	L_7 (nH)	R_8 (Ω)
Value	3.52	0.13	68.01	2.17	0.16	75.80
Circuit parameters	C_8 (pF)	L_8 (nH)				
Value	5.54	0.046				

to this figure, it is evident that decreasing the feed line width "W_f" from the proposed value of 3.95 mm to 3.55 mm results in a decrease in the impedance matching of the patch and the loss of UWB operation. Similarly, when "W_f" varies from 3.95 mm to 4.15 mm, it is observable that the antenna matching is reduced, and UWB operation is lost. Thus, it is concluded that $W_f = 3.95$ mm is the optimal value to achieve good matching and cover the [2.5–11.1] GHz band, subsequently achieving UWB operation with the best impedance matching. The "W_f" strongly influences the antenna's impedance matching and UWB performance by controlling the characteristic impedance of the microstrip line and shaping the current distribution at the feed. A narrow "W_f" yields a higher impedance than 50 Ω, while an excessively wide W_f results in a lower impedance, and both cases create mismatches that increase reflections and degrade return loss. When properly optimized, "W_f" ensures that the feed line impedance is well-matched to the antenna input impedance, thereby maximizing power transfer and minimizing losses. For UWB operation, this optimization is particularly important, as it stabilizes the impedance across the wide frequency spectrum, mitigates frequency-dependent mismatches, and promotes consistent excitation of the radiating patch. As a result, the antenna achieves efficient broadband. These adjustments optimize the integration of slots at the resonator's performance with improved return loss, wide bandwidth, and stable radiation characteristics throughout the UWB range.

2.4.2. Influence of Ground Plane Length (L_3)

Then, the second parameter studied is "L_3". The influence of this parameter on S_{11} is illustrated in Fig. 6(b), keeping

the other dimensions unchanged. According to Fig. 6(b), it is clear that after a gradual decrease of 1 mm in the length of the ground plane from the value used in the suggested patch ($L_3 = 13.25$ mm), the adaptation level of the S_{11} L_3 diagram is degraded, thus leading to multi-band operation with a narrow bandwidth. Furthermore, when the value of "L_3" is increased by 1 mm (L_3 becomes equal to 14.25), the impedance adaptation of the antenna is reduced, achieving multi-band operation but not reaching UWB operation. In conclusion, it is noted that a slight variation in "L_3" has a significant influence on the bandwidth and impedance adaptation of the antenna, and $L_3 = 13.25$ is the optimal value for achieving UWB operation. Adjusting the length of the ground plane "L_3" significantly affects both the bandwidth and impedance matching of the antenna, which is critical for achieving ultra-wideband (UWB) operational. A well-chosen ground plane length helps to control the current distribution and electromagnetic field coupling between the antenna and the ground, both of which influence the antenna's impedance characteristics across a wide frequency range. By increasing or decreasing "L_3", designers can effectively tune the lower- and upper-frequency bounds of the operational band, thereby enhancing or limiting the bandwidth. Adjusting "L_3" helps to achieve better impedance matching by minimizing return losses across the desired frequency range, thereby reducing reflections and maximizing energy transfer, both of which are essential for stable UWB performance.

2.4.3. Effect of the Radius (R) of the Resonator

This section delves into the variations in radius "R" of the resonator, a crucial element in the design, aimed at evaluating its impact on the S_{11} properties of the proposed patch. It represents the third major design factor examined in this section. Changes in simulated S_{11}, achieved by varying the "R" parameter, are depicted in Fig. 6(c) to illustrate its influence on S_{11}. From Fig. 6, it is evident that the resonator's radius "R" significantly affects the operating band. However, due to fluctuations in the "R" value, the performance of the operational bandwidth diminishes. A minor variation in "R" on the order of 0.5 mm results in the loss of UWB functionality, consequently failing to cover the desired operating bands. A recommended radius of $R = 13$ mm enhances impedance matching for the proposed antenna, leading to an extended operational bandwidth of up to 8.60 GHz. In light of this, it can be affirmed that the proposed antenna attains optimal performance in terms of operational bandwidth and S_{11} when configured with a radius of R equal to 13 mm. The deterioration observed at certain radius values can indeed be attributed to changes in the current distribution on the patch surface. Specifically, when the radius is increased beyond the optimized value, the effective electrical length of the patch changes, which alters the resonant frequency and disrupts the matching condition. This results in a redistribution of surface currents, leading to degraded impedance matching and reduced radiation efficiency. Conversely, when the radius is reduced, the current paths shorten, limiting the effective radiation aperture and causing bandwidth narrowing. Additionally, adjusting "R" affects the antenna's S_{11} characteristics influencing the quality of resonance and minimizing return losses over the desired frequency range, which is crucial for achieving stability, and broad UWB performance. Thus, fine-tuning "R" allows designers to optimize the bandwidth and impedance matching to achieve efficient ultra-wideband operation.

2.4.4. Current Distributions Analysis

Parametric analyses have revealed that adjusting parameters such as feed line width "W_f", ground plane length "L_3, and resonator radius "R" generates an ultra-wide bandwidth. As illustrated in Fig. 7, the current distribution on the patch accounts for this observation, highlighting seven resonance frequencies at 2.94 GHz, 3.47 GHz, 4.34 GHz, 6.05 GHz, 7.35 GHz, 8.92 GHz, and 9.72 GHz. They can also explain the influence of the "E" and inverted "E" shaped slots in resonators and the slots at the ground plane on the generation of UWB operation.

Analyzing Figs. 7(a), (b), (c), and (d), a noteworthy concentration of current is observed at the resonator and ground plane slots, leading to the creation of the operating band with improved antenna electrical performances at low-frequency operating bands, and subsequently ensure proper operation for applications such as WLAN, WiMAX, Bluetooth, Wi-Fi, and the ITU. The surface currents depicted in Fig. 7(e) demonstrate exceptional spreading across all parts of the antenna, resulting in optimal radiation and, consequently, effective operation in the X-band. Similarly, in both Figs. 7(f) and (g), surface currents concentrate more on the slots located at the resonator and ground plane below the feed line, resulting in a bandwidth covering the C, X, and ITU-assigned amateur radio bands.

3. RESULTS AND DISCUSSION

HFSS software was utilized for the design and optimization of the antenna. Subsequently, the fabrication and measurement of the parameters of the suggested optimal patch were carried out to validate the simulated results. Figs. 8(a), (b), and (c) depict the front and rear views of the manufactured antenna, along with its measurement setup in the anechoic chamber.

The antenna was tested using a National Instruments vector network analyzer. The measured results demonstrated a 90% correlation with the simulated data, attributed to the highly precise fabrication process, which was repeated multiple times to achieve optimal alignment with the simulation outcomes.

The S_{11} is a crucial parameter for delineating the operational frequency ranges of the antenna. The network analyzer was employed to measure the S_{11}, and the measured results were compared to those obtained through simulation (using HFSS). The comparative results are depicted in Fig. 9. As shown in Fig. 9, a notable agreement between simulated and experimental results is observed for the bandwidth when S_{11} is less than -10 dB. It can be inferred from this figure that the measured results align well with the simulated values. However, the reflection loss graph of the experimental results shows an improvement in the low-frequency range and a slight deviation after the 10.3 GHz frequency. This discrepancy, where impedance matching decreases, can be attributed to SMA connector losses, manufacturing tolerances, FR-4 substrate losses (especially at higher frequencies), and the measurement environment. Upon

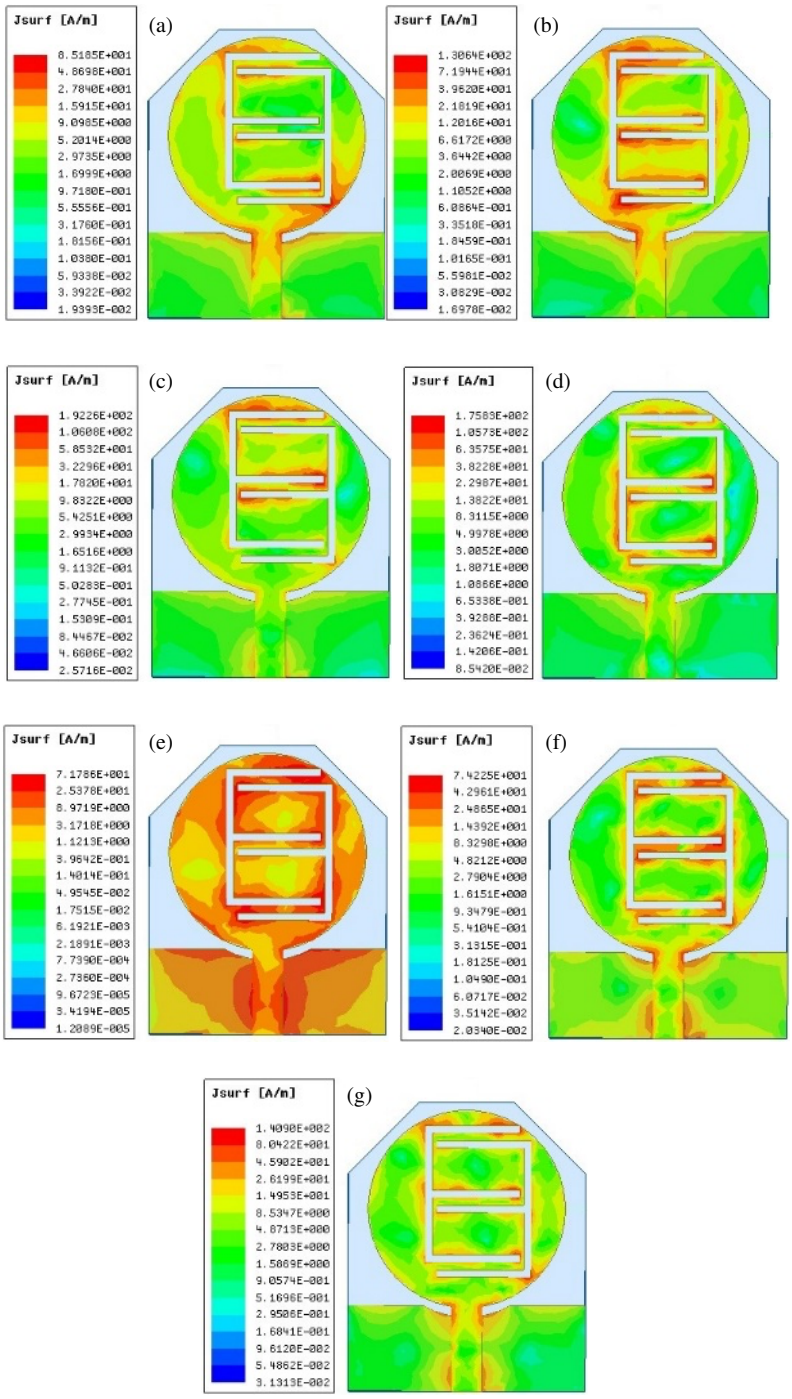

FIGURE 7. Simulated current distributions at (a) 2.93 GHz, (b) 3.47 GHz, (c) 4.34 GHz, (d) 6.05 GHz, (e) 7.35 GHz, (f) 8.92 GHz, (g) 9.72 GHz.

examining the experimental results illustrated in Fig. 9, it can be affirmed that the operation in ultra-wideband (UWB) is confirmed. Furthermore, the fabricated prototype can cover the frequency range [2.1–2.16] GHz, [2.48–10.48] GHz, and [11.23–12] GHz, with a measured bandwidth of 0.06, 10, and 0.77 GHz, representing 97.18% of the entire tested frequency range.

The radiation properties of the proposed antenna were examined and presented in terms of radiation efficiency, radiation pattern, and peak gain. The simulation results were validated by experimental measurements in an anechoic chamber as shown in Fig. 8(c).

Figures 10, 11, and 12 illustrate the simulated and measured results of the 2D radiation pattern, peak gain, and radiation efficiency of the proposed antenna. The results obtained from simulation and measurement of the 2D radiation pattern show excellent agreement with slight disparities. Fig. 10 demonstrates that the fabricated antenna effectively radiates across the entire operating band. The radiation pattern in the H-plane for the first three resonance frequencies exhibits omnidirectional

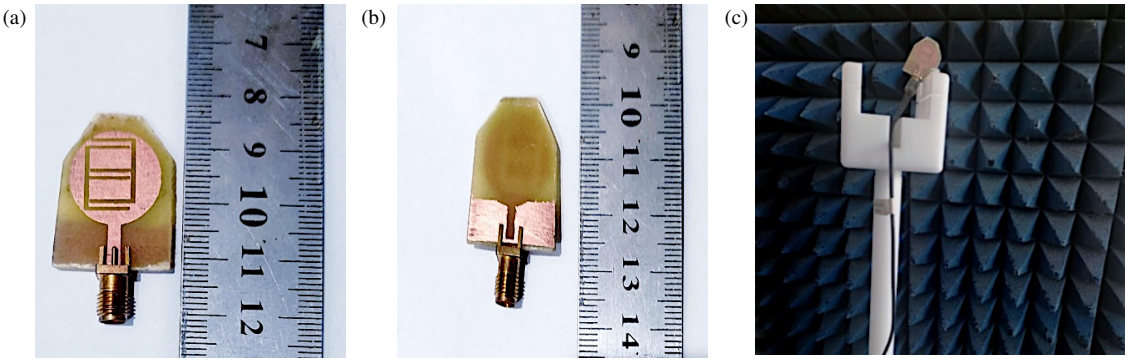

FIGURE 8. Prototype patch antenna. (a) View from the top, (b) view from the bottom, and (c) setup for measuring radiation characteristics in the anechoic chamber.

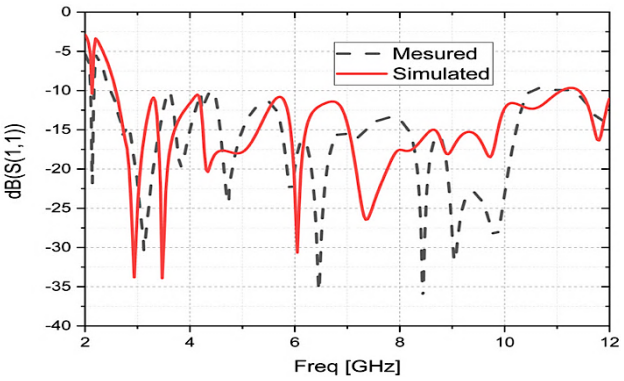

FIGURE 9. S_{11} (dB) of the antenna under simulation and actual measurement.

radiation, while it becomes quasi-omnidirectional at other resonance frequencies. The antenna radiation pattern in the E-plane adopts an "8" shape (bidirectional) at the three lowest resonant frequencies and becomes quasi-omnidirectional at other frequencies. The observed modification in the radiation pattern at high frequencies is due to the influence of the FR-4 substrate's characteristics at these frequencies. High-frequency effects, such as increased dielectric losses and dispersion within the FR-4 material, alter the propagation and distribution of electromagnetic fields, leading to a change in the antenna's radiation pattern. A slight disparity is observed in Fig. 11 between the measured and simulated peak gains. This difference may be attributed to manual soldering, the presence of impurities in the substrate used for fabrication, or connector effects. Additionally, it is noted that the peak gain increases with frequency. This observation could be explained by the dimensions of the antenna exceeding the wavelength as the frequency increases. The peak gain can reach 7.4 dB at the frequency of 11.23 GHz. The radiation efficiency of an antenna measures its ability to convert electrical energy into electromagnetic waves emitted into space. It represents the antenna's efficiency in transmitting or receiving signals with minimal losses. High radiation efficiency is sought to ensure optimal antenna performance. In other words, radiation efficiency quantifies how effectively an antenna converts received electrical energy into useful radiation while minimizing losses as heat or stored energy within the antenna structure. The simulated radiation efficiency of the proposed antenna can reach up to 98%. Additionally, the measured radiation efficiency of the prototype reached 97% at the frequency of 2.56 GHz.

Table 3 presents a comparison between the results of the proposed monopole antenna and those of the antennas presented recently in the literature [11–17] on UWB antennas in terms of area (mm^2), substrate type, operating range (GHz), peak gain (dB), and efficiency (%). The analysis reveals that the proposed monopole antenna outperforms previous designs, boasting a smaller footprint and superior performance. Specifically, the monopole antenna introduced in this paper demonstrates significant advantages over prior research. By leveraging an FR4 substrate, it achieves cost-effective manufacturing while maintaining a compact form factor of 1101.38 mm^2, an impressive impedance bandwidth, high efficiency, and a peak gain of 7.5 dB.

4. UWB-MIMO ANTENNA

A strong coupling is generated between antennas placed at a distance less than $\lambda/4$. This mutual interference can be mitigated by opting for antennas that have an appropriate separation distance within the mobile terminal. They can be positioned either with some on the upper side and the others on the lower side, or on the same side. This arrangement of antennas also disrupts the phase of coupling currents, compromising the polarization of the radiated fields. Reducing ground coupling and field coupling can be achieved by orienting adjacent antennas perpendicularly (at 90°). Orthogonally arranged linearly polarized antennas increase isolation and provide polarization diversity [29, 39]. The design addresses the challenge of requiring an intact floor in mobile terminal applications by employing several strategies to optimize performance despite floor interruptions. This strategy includes using a partial ground plane or ground slit, which adapts the antenna to non-continuous ground surfaces commonly found in compact mobile devices, thus maintaining impedance matching and operational bandwidth. Additionally, positioning the antenna near the edges of the terminal minimizes the impact of ground interruptions, allowing the antenna to function effectively even with a non-intact floor.

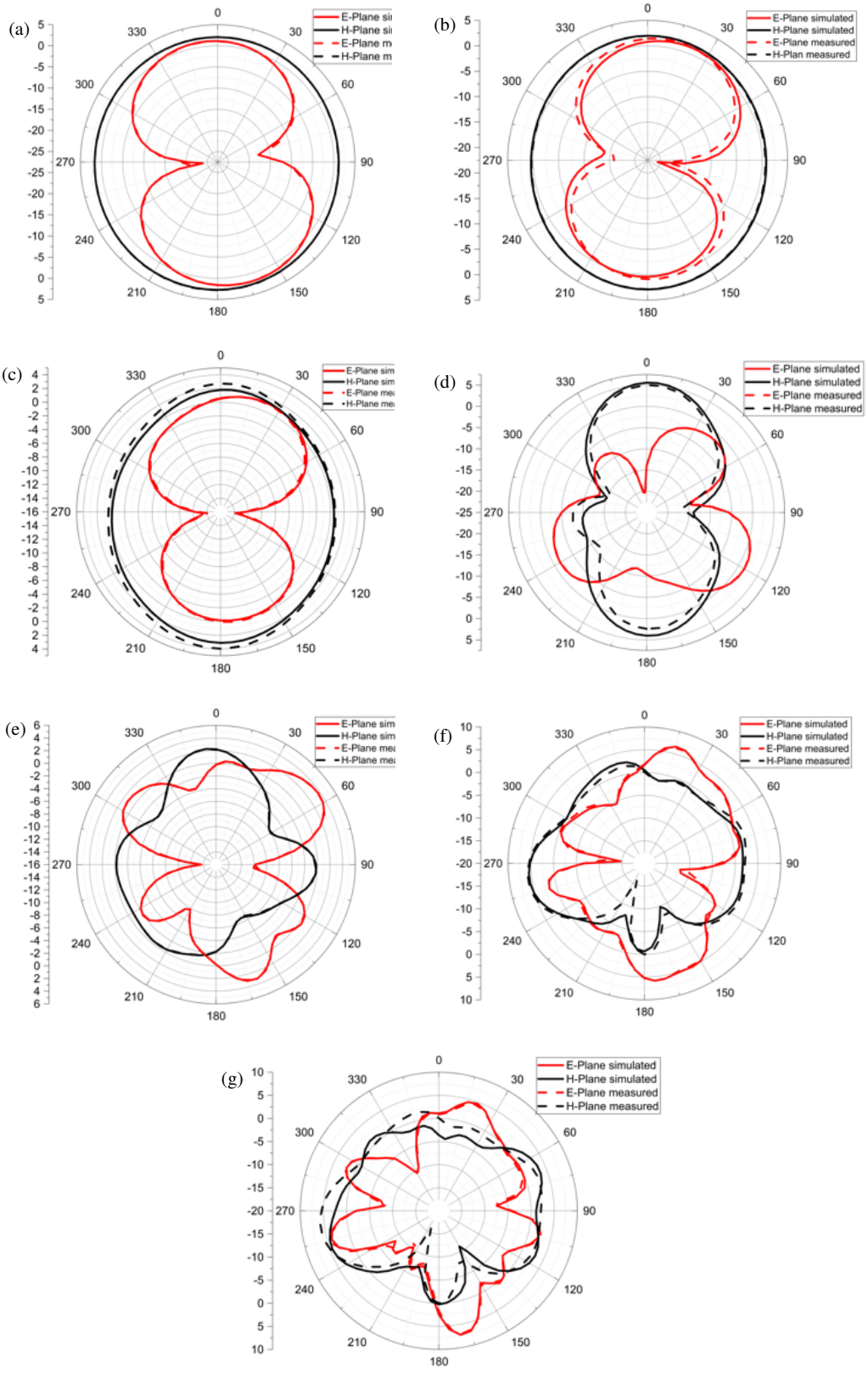

FIGURE 10. Radiation patterns in the E and H planes at (a) 2.93 GHz, (b) 3.47 GHz, (c) 4.34 GHz, (d) 6.05 GHz, (e) 7.35 GHz, (f) 8.92 GHz, (g) 9.72 GHz.

Various isolation methods for MIMO antenna systems have been documented in previous studies. In this section of the article, a new UWB-MIMO antenna with four elements, each identical to the one proposed in the first part, is introduced to further enhance its performance while operating within the UWB frequency range. The four monopoles are symmetrically

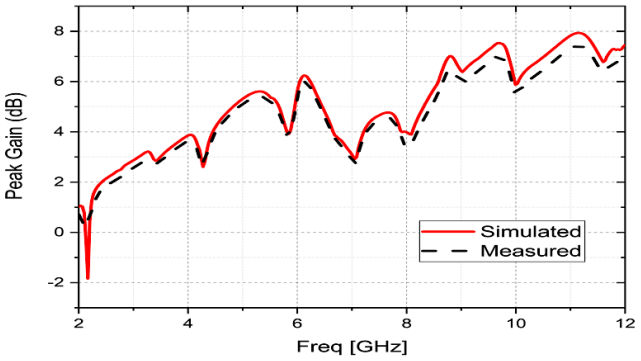

FIGURE 11. Simulated and measured peak gains.

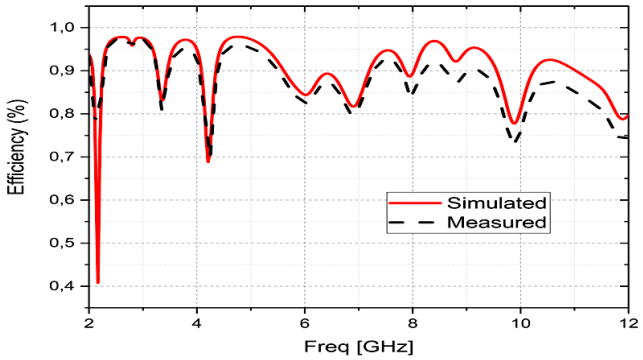

FIGURE 12. Simulated and measured radiation efficiencies.

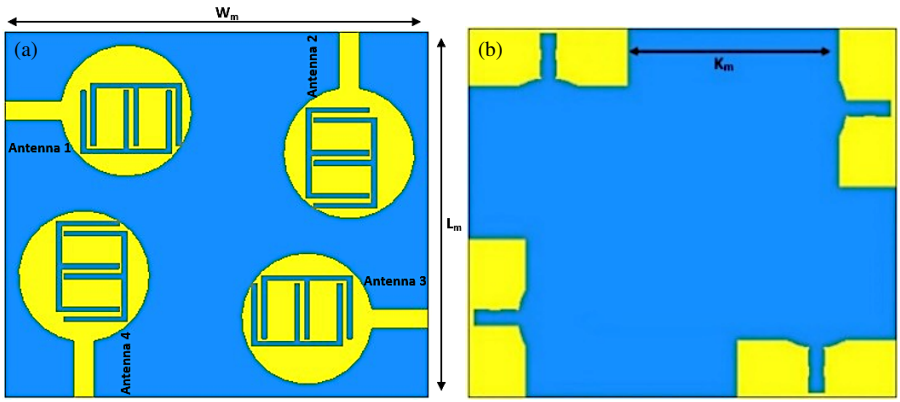

FIGURE 13. Suggested a circular-shaped MIMO antenna with unconnected ground, (a) frontal schematic view, (b) rear schematic view.

TABLE 3. Comparison of the proposed monopole patch with structures reported in previous studies.

Ref. No.	Area (mm^2)	Subs type	Operating range (GHz)	Peak gain (dB)	Efficiency (%)
[11]	75 × 63	Rogers RO4232	[3.10–10.6]	< 3.50	< 85
[12]	53 × 63.5	FR4	1.2–9.8	< 5.2	< 85
[13]	100 × 78	Taconic TLY-5	2-5	< 3	Not specified
[14]	40 × 30	FR4	3.4–7, 8–11.4	< 5	< 95
[15]	38.31 × 34.52	FR4	3.1–10.6	< 5	< 95
[16]	48 × 55	FR4	1.9–5, 6–10.6	< 5	Not specified
[17]	64 × 37.4	F4BM	1.5–10.4	< 2	Not specified
This work	1101.38	FR4	2.1–2.16, 2.48–10.48, 11.23–12	< 7.5	< 98

and orthogonally distributed on the upper part of the substrate, with the ground plane located on the lower side. The four elements of the MIMO antenna are arranged orthogonally in a stair-like pattern, separated, and mutually adjacent. This configuration aims to minimize the mutual coupling effect between the resonators. The simulated results of the suggested UWB-MIMO antenna are subsequently analyzed. Fig. 13 depicts the two-dimensional configuration of the four-element MIMO antenna proposed with unconnected ground elements. The antenna is designed on a cost-effective FR4 substrate with a thickness of 1.6 mm, a length of $W_m = 84$ mm, and a width of $L_m = 72.5$ mm. Figs. 14 and 15 depict, respectively, the layout of the MIMO antenna with the four ground elements connected and the comparison of S_{11} between the MIMO antenna with ground connected and that with ground unconnected. There is a slight difference in the performance of the antenna with or without connected ground. The reflection coefficient of the MIMO antenna with unconnected ground ensures the desired UWB operation with better adaptation. When the grounds are connected, strong surface currents couple between the antenna elements, leading to increased mutual coupling and deterioration of isolation performance. This effect was confirmed through S_{11} plots. The connected ground provides an unwanted coupling path, thereby reducing the isolation and overall sys-

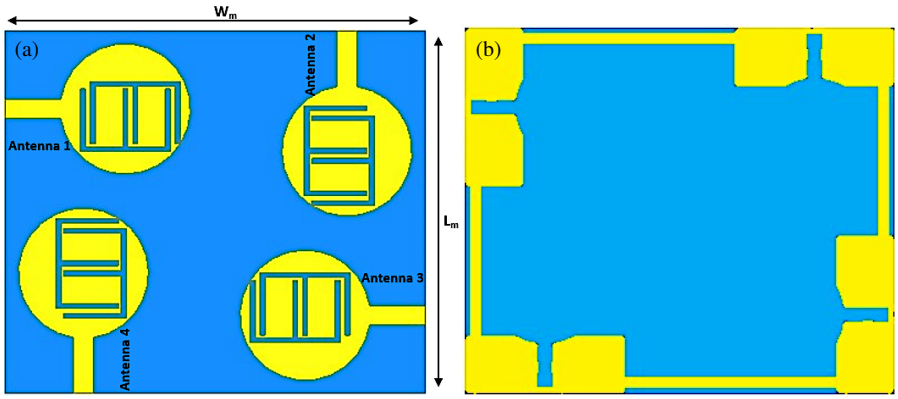

FIGURE 14. Suggested circular-shape MIMO antenna with common ground, (a) frontal schematic view, (b) rear schematic view.

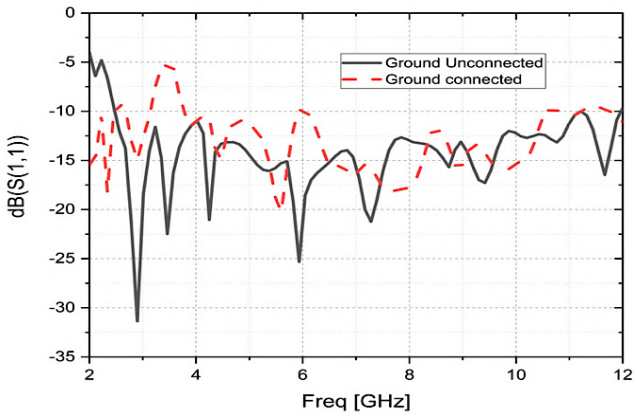

FIGURE 15. Comparison of S_{11} between the MIMO antenna with connected ground and the one with disconnected ground.

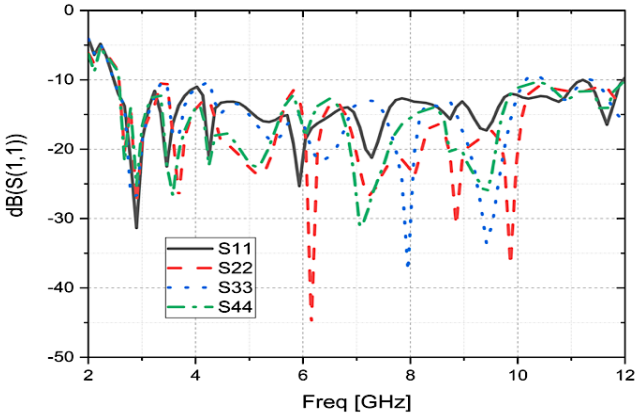

FIGURE 16. Simulated S-parameters of the MIMO antenna.

tem performance. Compared to conventional UWB-MIMO designs, the proposed antenna achieves improved isolation and stable radiation characteristics with a relatively simple geometry, making it well-suited for practical wireless devices. In the subsequent sections of the article, we will discuss the performance of the MIMO antenna with unconnected ground elements.

The simulation plots depicting the reflection coefficients of the UWB MIMO antenna across various ports (S_{11}, S_{22}, S_{33}, S_{44}) are illustrated in Fig. 16. Analysis of the simulated response reveals that the antenna exhibits an impedance bandwidth of -10 dB ranging from 2.47 GHz to 12 GHz, with a width of 9.53 GHz. This study highlights that the utilization of the four-port MIMO antenna significantly enhances both adaptation and bandwidth compared to the monopole antenna employed. This improvement grants the antenna an extended capability to cover applications such as WLAN (2.4–2.484 GHz), Wi-MAX (2.5–2.69 GHz), LTE (2.5–2.69 GHz), Bluetooth (2.47–2.4835 GHz), and Wi-Fi (2.47–2.49 GHz). Consequently, the UWB MIMO antenna emerges as a versatile solution for a broad range of wireless applications.

Figures 17(a) and (b) highlight the mutual coupling between different resonant elements of the MIMO antenna. This inter-element coupling has been minimized through an orthogonal arrangement of resonant elements and by maintaining a distance between unconnected portions of the ground plane. Isolation of over 22.4 dB has been achieved across the entire operating bandwidth, as demonstrated in Fig. 17. Additionally, a peak gain ranging between 4.14 and 11.57 dB has been obtained, covering the entire bandwidth, as shown on Fig. 18.

The antenna envelope correlation coefficient (ECC) assesses the similarity in amplitudes of signals emitted by different antennas in a system. A coefficient close to 1 suggests a strong correlation, which may be less favorable in MIMO systems. Conversely, a coefficient close to 0 indicates a low correlation, promoting a more independent contribution of antennas to enhance the reliability and performance of wireless communications. It's worth noting that, the ECC is computed utilizing the methodology outlined in [40] for a lossless MIMO antenna. The ECC for a four-port MIMO system among antenna elements is formulated by (4).

Figure 19 illustrates the plot of the ECC among the various elements of a four-port MIMO system. It is observed that the ECC remains below 0.014 across the entire UWB, ensuring excellent diversity performance for the MIMO antenna. The simulated two-dimensional radiation pattern of the proposed MIMO antenna in both planes E and H at 2.90, 3.46, 4.25, 5.93, 7.28, 9.42, and 11.66 GHz frequencies are shown

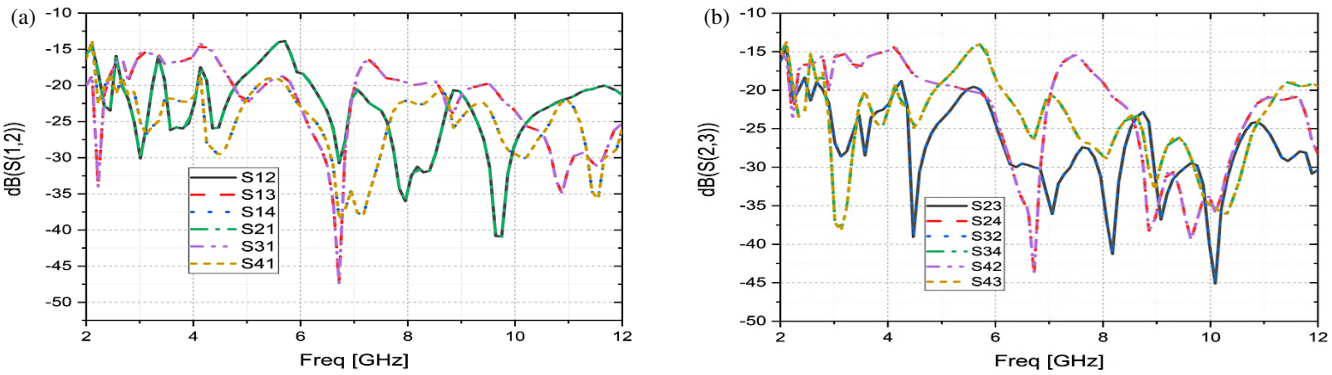

FIGURE 17. Simulated S-parameters of the UWB MIMO antenna. (a) Port 1, (b) other ports.

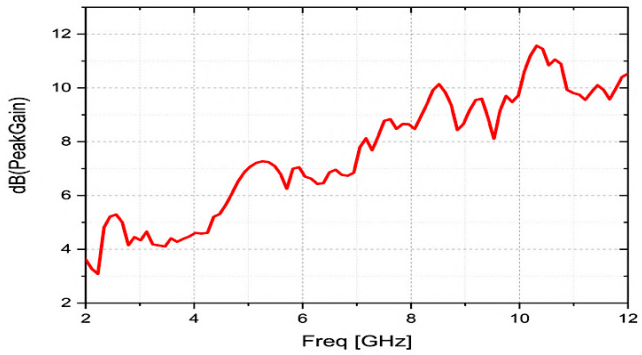

FIGURE 18. Peak gain of the UWB MIMO antenna.

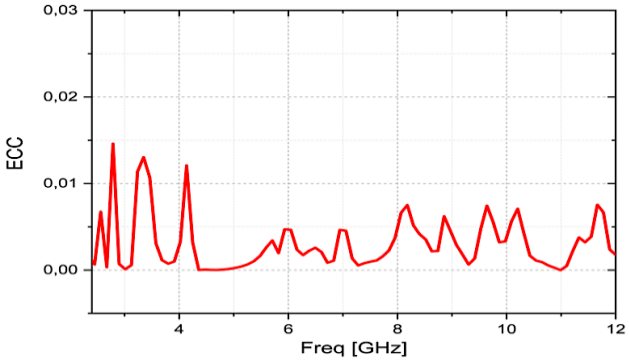

FIGURE 19. ECC for the UWB MIMO patch antenna.

TABLE 4. Proposed UWB-MIMO performance comparison with MIMO antennas presented in the literature.

Ref. No.	Area (mm^2)	Subs type	Operating range (GHz)	Peak gain (dB)	Isolation (dB)	ECC
[30]	154×154	FR4	-	< 5	> 40	-
[31]	145×75	FR4	3.4–3.6	< 4.5	> 15	< 0.16
[32]	150×75	FR4	3.4–3.6	< 1.6	> 20	< 0.3
[33]	263×263	FR4		< 7	18	0.16
[34]	24×22	FR4	3.37–5.64	NA	15	< 0.04
[35]	150×75	FR4	3.4–3.6, 4.8–5.0	< 5.1	16.5	< 0.01
This work	84×72.5	FR4	2.47–12	< 12	> 22.4	< 0.01

$$\rho_e\left(1,2,4\right) = \frac{\left|S_{11}^* S_{12} + S_{21}^* S_{22} + S_{13}^* S_{32} + S_{14}^* S_{42}\right|^2}{\left(1 - \left|S_{11}\right|^2 - \left|S_{21}\right|^2 - \left|S_{31}\right|^2 - \left|S_{41}\right|^2\right)\left(1 - \left|S_{12}\right|^2 - \left|S_{22}\right|^2 - \left|S_{32}\right|^2 - \left|S_{42}\right|^2\right)} \tag{4}$$

in Fig. 20. In Fig. 20, it can be observed that in the H-plane, the radiation pattern of the antenna is omnidirectional at the first two resonance frequencies, becoming approximately omnidirectional at the other resonance frequencies. This evolution is attributed to the impact of higher frequencies on the behavior of the FR-4 substrate. Additionally, it is noteworthy that for the first three resonance frequencies, the radiation pattern in the E-plane takes on an "8" shape, indicating bidirectional radiation. For the other resonance frequencies, it demonstrates quasi-omnidirectional operation.

Table 4 provides a comparison between the proposed UWB-MIMO and other UWB-MIMO antennas published in recent years. While not exhaustive, this comparison effectively captures the current state-of-the-art in UWB-MIMO technology. The comparison table highlights the numerous advantages of the proposed MIMO antenna over the referenced antennas [30–35]. Particularly, it distinguishes itself in terms of size, operating range, gain, isolation, and ECC. The proposed technique, utilizing a stair-shaped pattern coupled with a defective ground structure left unconnected to reduce mutual coupling, proves to be both simple and effective. The results demonstrate that the

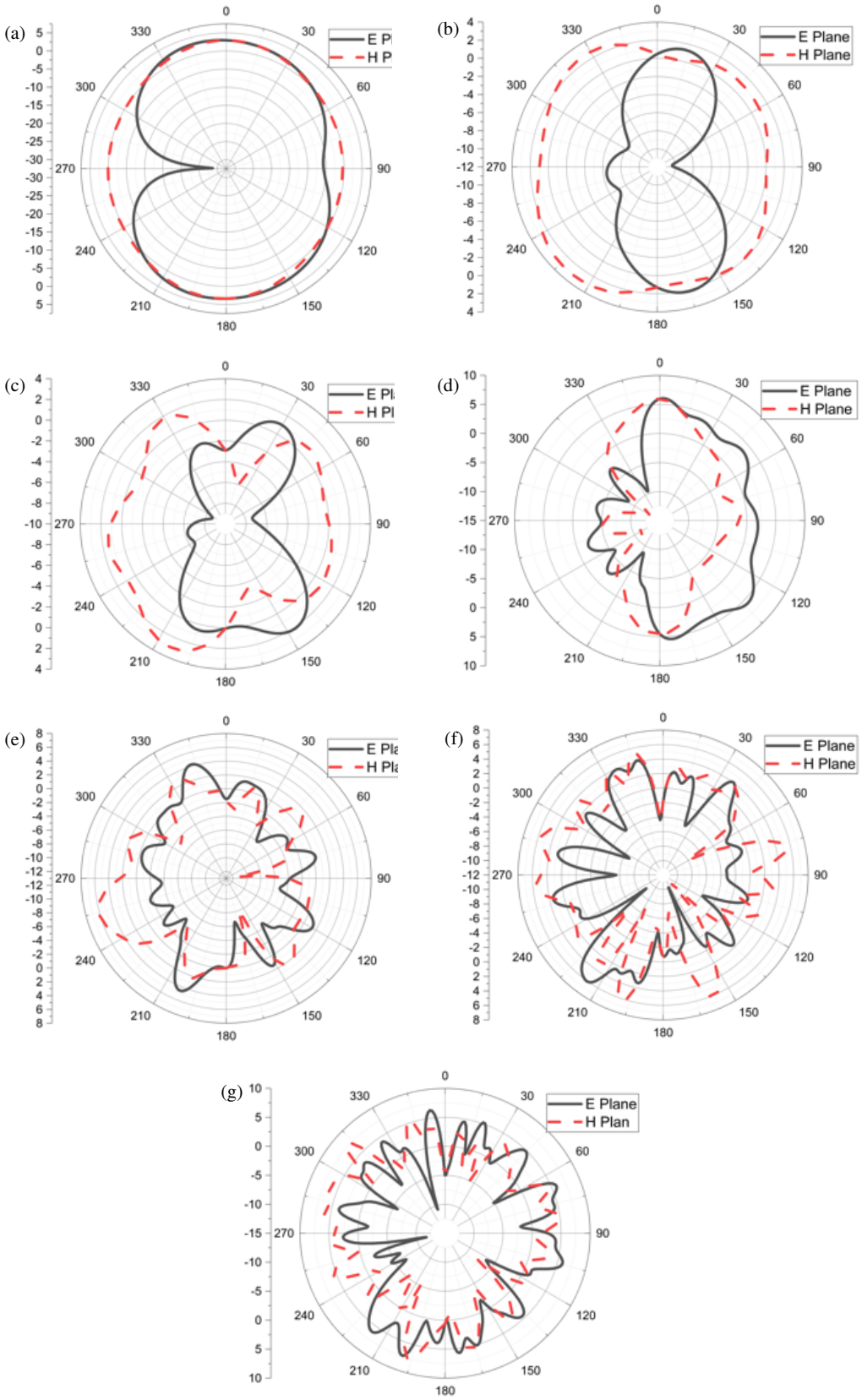

FIGURE 20. Two-dimensional radiation pattern of the proposed MIMO antenna, (a) 2.90 GHz, (b) 3.46 GHz, (c) 4.25 GHz, (d) 5.93 GHz, (e) 7.28 GHz, (f) 9.42 GHz, (g) 11.66 GHz.

proposed antenna strikes an excellent balance in terms of size, operating range, gain, isolation, and ECC. The designed MIMO antenna covers the impedance spectrum from 2.42 to 12 GHz, with a gain reaching 12.77 dB and efficiency reaching 98%, as well as isolation of over 22.4 dB and an ECC of less than 0.014 across the entire operating bandwidth.

5. CONCLUSION

To provide a typical solution for short-range wireless communications and transmit signals across a wide range of frequencies with low power consumption in transmission and reception, this article introduces two UWB antennas: the first is a unipolar antenna, and the second is a MIMO antenna. The design process of both antennas includes the use of the HFSS software to model and analyze the design before fabrication. The UWB monopole antenna was fabricated by machining the resonator onto a low-cost FR4 substrate with a volume of $1,101.38\,\text{mm}^2 \times 1.6\,\text{mm}$. Its ability to offer an extended impedance bandwidth is due to the use of two deformed "E" and "inverted E" slots on the patch, an irregular hexagonal substrate structure, and a partial ground plane composed of slots. The manufactured UWB antenna covers frequency ranges of [2.1–2.16] GHz, [2.48–10.48] GHz, and [11.23–12] GHz, with a maximum gain reaching 7.4 dB and an efficiency reaching 97%. Strong agreement between simulated and measured results validates the effectiveness of this UWB antenna for its application in multi-band environments. The MIMO antenna, which improves the performance of the first proposed monopole antenna, is designed by symmetrically integrating four prototypes of the suggested antenna. To significantly reduce mutual coupling between antenna elements, a distinct, orthogonal, and symmetrical quad-directional stair-like structure is introduced. The new antenna covers the impedance spectrum from 2.42 to 12 GHz, with a gain reaching 12.77 dB and an efficiency reaching 98%, as well as a VSWR ranging between 1 and 2.

ACKNOWLEDGEMENT

The authors gratefully acknowledge the support provided Universiti Teknikal Malaysia Melaka (UTeM), the Centre for Research and Innovation Management (CRIM), and the Ministry of Higher Education Malaysia (MOHE).

REFERENCES

[1] FCC & ISED Canada Testing at D.L.S. DLS Electronic Systems, Inc n.d., https://www.dlsemc.com/fcc-ised-canada-testing-at-d-l-s/, February 2024.

[2] Bharadwaj, R. and S. K. Koul, "UWB channel analysis using hybrid antenna configuration for BAN localization applications," in *2019 IEEE Indian Conference on Antennas and Propogation (InCAP)*, 1–4, Ahmedabad, India, 2019.

[3] Ibrahim, I. M., A. J. A. Al-Gburi, Z. Zakaria, and H. A. Bakar, "Parametric study of modified U-shaped split ring resonator structure dimension at ultra-wide-band monopole antenna," *Journal of Telecommunication, Electronic and Computer Engineering (JTEC)*, Vol. 10, No. 2-5, 53–57, 2018.

[4] Kumar, A., G. Singh, M. K. Abdulhameed, S. R. Hashim, and A. J. A. Al-Gburi, "Development of fractal 5G MIMO antenna for sub 6 GHz wireless automotive applications," *Progress In Electromagnetics Research M*, Vol. 130, 121–128, 2024.

[5] Kannappan, L., S. K. Palaniswamy, L. Wang, M. Kanagasabai, S. Kumar, M. G. N. Alsath, and T. R. Rao, "Quad-port multi-service diversity antenna for automotive applications," *Sensors*, Vol. 21, No. 24, 8238, 2021.

[6] Al-Gburi, A. J. A., Z. Zakaria, M. Palandoken, I. M. Ibrahim, A. A. Althuwayb, S. Ahmad, and S. S. Al-Bawri, "Super compact UWB monopole antenna for small IoT devices," *Computers, Materials & Continua*, Vol. 73, No. 2, 2785–2799, 2022.

[7] Bharadwaj, R., S. Swaisaenyakorn, C. G. Parini, J. C. Batchelor, and A. Alomainy, "Impulse radio ultra-wideband communications for localization and tracking of human body and limbs movement for healthcare applications," *IEEE Transactions on Antennas and Propagation*, Vol. 65, No. 12, 7298–7309, 2017.

[8] Gao, Y., Y. Zheng, S. Diao, W.-D. Toh, C.-W. Ang, M. Je, and C.-H. Heng, "Low-power ultrawideband wireless telemetry transceiver for medical sensor applications," *IEEE Transactions on Biomedical Engineering*, Vol. 58, No. 3, 768–772, 2011.

[9] Saeidi, T., I. Ismail, W. P. Wen, A. R. H. Alhawari, and A. Mohammadi, "Ultra-wideband antennas for wireless communication applications," *International Journal of Antennas and Propagation*, Vol. 2019, No. 1, 7918765, 2019.

[10] Doddipalli, S. and A. Kothari, "Compact UWB antenna with integrated triple notch bands for WBAN applications," *IEEE Access*, Vol. 7, 183–190, 2019.

[11] Das, S., H. Islam, T. Bose, and N. Gupta, "Ultra wide band CPW-fed circularly polarized microstrip antenna for wearable applications," *Wireless Personal Communications*, Vol. 108, No. 1, 87–106, 2019.

[12] Li, X.-P., G. Xu, C.-J. Duan, M.-R. Ma, S.-E. Shi, and W. Li, "Compact TSA with anti-spiral shape and lumped resistors for UWB applications," *Micromachines*, Vol. 12, No. 9, 1029, 2021.

[13] Delphine, A., M. R. Hamid, N. Seman, and M. Himdi, "Broadband cloverleaf Vivaldi antenna with beam tilt characteristics," *International Journal of RF and Microwave Computer-Aided Engineering*, Vol. 30, No. 5, e22158, 2020.

[14] Yeboah-Akowuah, B., E. T. Tchao, M. Ur-Rehman, M. M. Khan, and S. Ahmad, "Study of a printed split-ring monopole for dual-spectrum communications," *Heliyon*, Vol. 7, No. 9, e07928, 2021.

[15] Saritha, V., V. N. K. R. Devana, M. B. Lakshmi, M. A. Halimi, G. Devi, N. R. Lavuri, and A. J. A. Al-Gburi, "Low-profile four-port MIMO antenna realizing penta-band notches for UWB systems," *Optik*, Vol. 336, 172454, 2025.

[16] Chaudhary, P. and A. Kumar, "Compact ultra-wideband circularly polarized CPW-fed monopole antenna," *AEU — International Journal of Electronics and Communications*, Vol. 107, 137–145, 2019.

[17] Alam, M. S. and A. Abbosh, "Reconfigurable band-rejection antenna for ultra-wideband applications," *IET Microwaves, Antennas & Propagation*, Vol. 12, No. 2, 195–202, 2018.

[18] Al Gburi, A. J. A., "5G MIMO antenna: Compact design at 28/38 GHz with metamaterial and SAR analysis for mobile phones," *Przegląd Elektrotechniczny*, Vol. 100, No. 4, 171–174, 2024.

[19] Khan, A., S. Bashir, S. Ghafoor, and K. K. Qureshi, "Mutual coupling reduction using ground stub and EBG in a compact wideband MIMO-antenna," *IEEE Access*, Vol. 9, 40 972–40 979, 2021.

[20] Elabd, R. H. and A. J. A. Al-Gburi, "Low mutual coupling miniaturized dual-band quad-port MIMO antenna array using decoupling structure for 5G smartphones," *Discover Applied Sciences*,

Vol. 6, No. 4, 189, 2024.

[21] Kumar, P., A. K. Singh, R. Kumar, S. K. Mahto, P. Pal, R. Sinha, A. Choubey, and A. J. A. Al-Gburi, "Design and analysis of low profile stepped feedline with dual circular patch MIMO antenna and stub loaded partial ground plane for wireless applications," *Progress In Electromagnetics Research C*, Vol. 140, 135–144, 2024.

[22] Kaur, N., J. S. Sivia, and M. Kumar, "SRR and rectangular stubs loaded novel fractal antenna realization for multiband wireless applications," *Wireless Personal Communications*, Vol. 120, No. 1, 515–533, 2021.

[23] Sakli, H., C. Abdelhamid, C. Essid, and N. Sakli, "Metamaterial-based antenna performance enhancement for MIMO system applications," *IEEE Access*, Vol. 9, 38 546–38 556, 2021.

[24] Paul, P. M., K. Kandasamy, and M. S. Sharawi, "A multi-band U-strip and SRR loaded slot antenna with circular polarization characteristics," *Advanced Electromagnetics*, Vol. 9, No. 1, 41–48, 2020.

[25] Srivastava, K., S. Kumar, B. K. Kanaujia, and S. Dwari, "Design and packaging of ultra-wideband multiple-input-multiple-output/diversity antenna for wireless applications," *International Journal of RF and Microwave Computer-Aided Engineering*, Vol. 30, No. 10, e22357, 2020.

[26] Maurya, N. K. and R. Bhattacharya, "Design of compact dual-polarized multiband MIMO antenna using near-field for IoT," *AEU — International Journal of Electronics and Communications*, Vol. 117, 153091, 2020.

[27] Iqbal, A., O. A. Saraereh, A. W. Ahmad, and S. Bashir, "Mutual coupling reduction using F-shaped stubs in UWB-MIMO antenna," *IEEE Access*, Vol. 6, 2755–2759, 2018.

[28] Chandel, R., A. K. Gautam, and K. Rambabu, "Design and packaging of an eye-shaped multiple-input-multiple-output antenna with high isolation for wireless UWB applications," *IEEE Transactions on Components, Packaging and Manufacturing Technology*, Vol. 8, No. 4, 635–642, 2018.

[29] Tang, Z., X. Wu, J. Zhan, S. Hu, Z. Xi, and Y. Liu, "Compact UWB-MIMO antenna with high isolation and triple band-notched characteristics," *IEEE Access*, Vol. 7, 19 856–19 865, 2019.

[30] Khaleel, H. R., H. M. Al-Rizzo, A. Abbosh, and S. Abushamleh, "Printed Yagi-Uda array for MIMO systems," in *2013 IEEE Antennas and Propagation Society International Symposium (APSURSI)*, 1802–1803, Orlando, FL, USA, 2013.

[31] Liu, Y., A. Ren, H. Liu, H. Wang, and C.-Y.-D. Sim, "Eight-port MIMO array using characteristic mode theory for 5G smartphone applications," *IEEE Access*, Vol. 7, 45 679–45 692, 2019.

[32] Li, R., Z. Mo, H. Sun, X. Sun, and G. Du, "A low-profile and high-isolated MIMO antenna for 5G mobile terminal," *Micromachines*, Vol. 11, No. 4, 360, 2020.

[33] Jehangir, S. S. and M. S. Sharawi, "A novel dual wideband circular quasi-Yagi MIMO antenna system with loop excitation," *Microwave and Optical Technology Letters*, Vol. 58, No. 11, 2769–2774, 2016.

[34] Singh, A. K., S. K. Mahto, and R. Sinha, "A compact quad element MIMO antenna for LTE/5G (sub-6 GHz) applications," *Frequenz*, Vol. 77, No. 3-4, 173–183, 2023.

[35] Huang, J., G. Dong, J. Cai, H. Li, and G. Liu, "A quad-port dual-band MIMO antenna array for 5G smartphone applications," *Electronics*, Vol. 10, No. 5, 542, 2021.

[36] Balanis, C. A., *Antenna Theory: Analysis and Design*, John Wiley & Sons, 2016.

[37] Pele, I., A. Chousseaud, and S. Toutain, "Simultaneous modeling of impedance and radiation pattern antenna for UWB pulse modulation," in *IEEE Antennas and Propagation Society Symposium, 2004*, Vol. 2, 1871–1874, Monterey, CA, USA, 2004.

[38] Ansarizadeh, M., A. Ghorbani, and R. A. Abd-Alhameed, "An approach to equivalent circuit modeling of rectangular microstrip antennas," *Progress In Electromagnetics Research B*, Vol. 8, 77–86, 2008.

[39] Liu, L., S. W. Cheung, and T. I. Yuk, "Compact MIMO antenna for portable UWB applications with band-notched characteristic," *IEEE Transactions on Antennas and Propagation*, Vol. 63, No. 5, 1917–1924, 2015.

[40] Blanch, S., J. Romeu, and I. Corbella, "Exact representation of antenna system diversity performance from input parameter description," *Electronics Letters*, Vol. 39, No. 9, 705–707, 2003.